A Large-Signal Switching MESFET Model for Intermodulation Distortion Analysis

Kohei Fujii, Yasuhiko Hara, Toshiyuki Yakabe, *Member, IEEE*, and Hatsuo Yabe, *Member, IEEE*

***Abstract*—This paper describes an improved large-signal model for predicting an intermodulation distortion (IMD) power characteristic of MESFET's in switching applications. The model is capable of modeling the voltage-dependent drain current and its derivatives, including gate–source and gate–drain capacitors. The drain current and its derivatives are described by a function of a voltage-dependent drain conductance. The model parameters are extracted from a measured drain conductance versus gate voltage characteristic of an MESFET. This paper also presents a new fully symmetric equivalent circuit for switching MESFET's. The IMD power characteristics calculated with the use of the proposed method are compared with experimental data taken from a monolithic-microwave integrated-circuit single-pole double-throw switch. Good agreements over the large gate voltages and input power levels are observed.**

***Index Terms*—Harmonic distortion, MESFET's, nonlinear model, nonlinearities.**

I. Introduction

THERE IS A growing need for high-performance monolithic-microwave integrated-circuit (MMIC) control circuits such as switches, attenuators, phase shifters, and resistive mixers. These MMIC's have been realized by the use of MESFET's as switching elements. The intermodulation distortion (IMD) generated by MESFET's is one of the important performance characteristics that must be addressed in many switching applications. Therefore, to analyze the IMD power characteristics of MESFET's, a large-signal model for switching MESFET's must be developed. For this purpose, a simple model was proposed [1]; however, the model neglects a drain voltage dependency of the drain current $I_{\rm ds}$. It was shown recently that not only the voltage-dependent $I_{\rm ds}$, but also their derivatives have to be modeled correctly, especially if the model is supposed to predict the IMD power characteristic [2], [3]. In those papers, the $I_{\rm ds}$ and its derivatives are accurately represented by the Taylor series expansion. Numerical calculation of the derivatives from the measured $I_{\rm ds}(V_{\rm gs}, V_{\rm ds})$ data is impractical because the MESFET's drain current is very small and its nonlinearity is often lost within measured tolerances. Therefore, the method requires a very complicated measurement procedure to extract the Taylor-series expansion coefficients.

Manuscript received January 25, 1999; revised December 10, 1999.

K. Fujii and Y. Hara are with the Japan Radio Company Ltd., Tokyo 181-8510, Japan (e-mail: fujii@tokki.jrc.co.jp).

T. Yakabe and H. Yabe are with the Department of Information and Communication Engineering, University of Electro-Communications, Tokyo 182-8585, Japan.

Publisher Item Identifier S 0018-9480(00)02051-2.

To overcome this problem, this paper presents a different approach in large-signal modeling. First, we focus on a voltage-dependent drain conductance $G_{\rm ds}$, not on the $I_{\rm ds}$, to describe the drain current. Second, the Taylor series coefficients are numerically extracted from the measured $G_{\rm ds}(V_{\rm gs}, V_{\rm ds})$ data. Finally, we propose a fully symmetrical equivalent circuit and an improved modeling function.

The paper is organized as follows. Section II begins with a nonlinear drain current for switching MESFET's. Section III shows problems of conventional models. Section IV continues with design of modeling functions. Section V shows an application example for predicting the IMD power performances of an MMIC single-pole double-throw (SPDT) switch.

II. Voltage-Dependent Drain Current for Switching MESFET's

In switching applications, an MESFET is controlled by a control dc gate voltage $V_{\rm gs}$, and a small-signal voltage $v_{\rm ds}$ applies to the drain at the zero drain bias voltage $V_{\rm ds}$. Under the condition, the small-signal drain current $i_{\rm ds}$ is described as a function of the voltage-dependent drain conductance and its derivatives

$$\begin{aligned} &i_{\rm ds}(V_{\rm gs}, V_{\rm ds}+v_{\rm ds}) \\ &\quad = G_{\rm ds}(V_{\rm gs}, V_{\rm ds})v_{\rm ds} + \frac{1}{2}\frac{\partial G_{\rm ds}(V_{\rm gs}, V_{\rm ds})}{\partial V_{\rm ds}}v_{\rm ds}^2 \\ &\qquad + \frac{1}{6}\frac{\partial^2 G_{\rm ds}(V_{\rm gs}, V_{\rm ds})}{\partial V_{\rm ds}^2}v_{\rm ds}^3 + \cdots \\ &\quad = g_1(V_{\rm gs}, V_{\rm ds})v_{\rm ds} + g_2(V_{\rm gs}, V_{\rm ds})v_{\rm ds}^2 \\ &\qquad + g_3(V_{\rm gs}, V_{\rm ds})v_{\rm ds}^3 + \cdots. \end{aligned} \tag{1}$$

The $G_{\rm ds}$ can be extracted accurately from measured S-parameters [4]. To extract equivalent element values of an MESFET from the S-parameters, we then propose a fully symmetrical large-signal equivalent circuit based on the physical configurations of switching MESFET's. Schematic cross sections at "on" and "off" states can be written by Fig. 1(a) and (b), respectively. The symmetrical equivalent circuit proposed here is shown in Fig. 2. The drain current is represented by a modeling function of the $G_{\rm ds}(V_{\rm gs}, V_{\rm ds})$. Since the drain is unbiased, and the MESFET is physically symmetrical, both a gate–source capacitor $C_{\rm gs}$ and a gate–drain capacitor $C_{\rm gd}$ have identical gate voltage dependencies. Parasitic elements R_g, R_d, R_s, L_g, L_d, L_s, and $C_{\rm ds}$ are assumed to be linear. The equivalent-circuit parameters can be extracted by using an optimization procedure to minimize an absolute square error between the measured and the modeled S-parameters. Parameter extraction of the equivalent circuit was done by GASMAP, Norwood, MA [5]. S-pa-

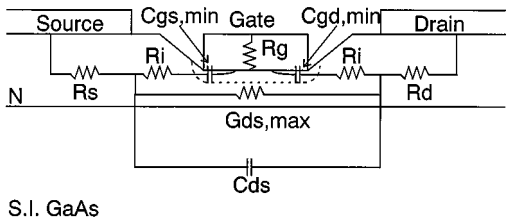

(a)

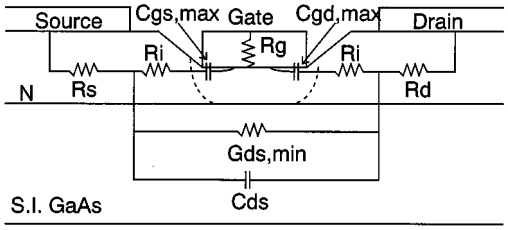

(b)

Fig. 1. Schematic cross section of a MESFET. (a) $V_{\rm gs} = 0$ V. (b) $V_{\rm gs} \ll V_p$.

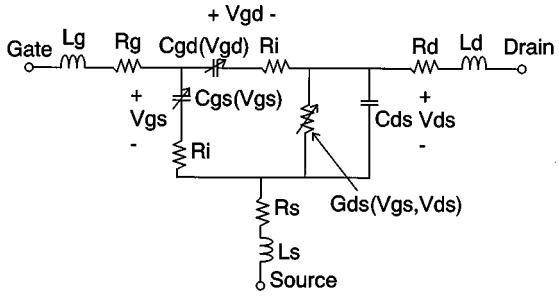

Fig. 2. Symmetrical equivalent circuit for a switching MESFET.

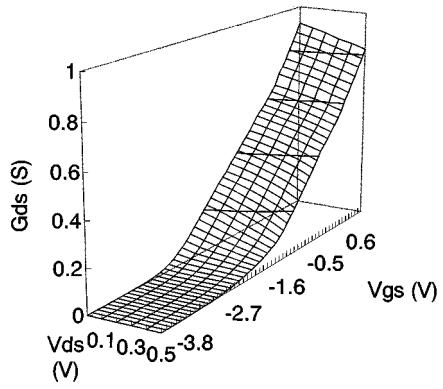

Fig. 3. A three-dimensional plot of the measured voltage dependent drain conductance for an 800-μm MESFET.

rameter measurements for the MESFET with 800-μm gatewidth were done from 1–21-GHz frequencies, and the measurement repeated the gate voltages over -5 to $+0.6$ V, and the drain voltages over 0–0.5 V. Fig. 3 shows measured $G_{\rm ds}(V_{\rm gs}, V_{\rm ds})$ data. From the $G_{\rm ds}(V_{\rm gs}, V_{\rm ds})$ data, the g_n, $n = 1, 2, 3, \cdots$ coefficients are numerically derived by using (1).

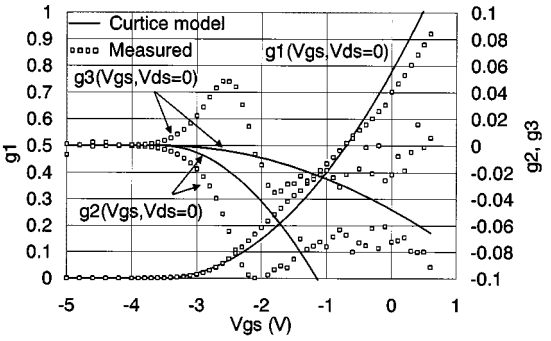

Fig. 4. Comparison of the measured and modeled g_n characteristics for an 800-μm MESFET. The parameters of the Curtice's modeling function are $\alpha = 0.647$, $\beta = 0.096$, $\lambda = -0.259$, and $V_p = -3.55$ V.

III. Problems of Conventional Modeling Functions

Many modeling functions for the large-signal model currently being used are mainly derived from the Curtice's modeling function [6]–[10]. The Curtice's modeling function is described by formulas

$$I_{\rm ds}(V_{\rm gs}, V_{\rm ds}) = \beta(V_{\rm gs} - V_p)^2(1 + \lambda V_{\rm ds})\tanh(\alpha V_{\rm ds}) \quad (2)$$

where $V_{\rm gs}$ and $V_{\rm ds}$ are the intrinsic terminal voltages, V_p is the pinchoff voltage, and α, β, and λ are the model parameters. For switching applications, (2) can be described as the voltage-dependent drain conductance

$$\begin{aligned} G_{\rm ds}(V_{\rm gs}, V_{\rm ds}) &= \frac{\partial I_{\rm ds}(V_{\rm gs}, V_{\rm ds})}{\partial V_{\rm ds}} \\ &= \beta(V_{\rm gs} - V_p)^2(1 + \lambda V_{\rm ds})\left\{\alpha \Big/ \left[\cosh^2(\alpha V_{\rm ds})\right]\right\} \\ &\quad + \beta(V_{\rm gs} - V_p)^2 \lambda \tanh(\alpha V_{\rm ds}). \end{aligned} \quad (3)$$

Equation (3) models the MESFET's $G_{\rm ds}$ adequately to obtain switch's isolation; however, (3) often fails the IMD power calculation. This shortage is clarified by a comparison of the g_n coefficients of a real device with those of the modeling function, as shown in Fig. 4. The comparison results show that the measured MESFET's coefficients vary with $V_{\rm gs}$ in progressively more complex manner as n increases; however, those of the Curtice's modeling function become simpler. From this comparison, it is considered that the large-signal simulation using the Curtice's modeling function causes the error of the IMD power. More sophisticated models [9], [10] also fail to represent the g_n coefficients because those models were developed to represent the I–V characteristics and those partial derivatives with respect to the gate voltage $V_{\rm gs}$.

IV. Improved Modeling Function

Conventional modeling functions being currently used [6]–[10] are expressed as

$$G_{\rm ds}(V_{\rm gs}, V_{\rm ds}) \approx F_1(V_{\rm gs}) \cdot F_2(V_{\rm ds}). \quad (4)$$

However, from the Fig. 3, the $G_{\rm ds}$ versus $V_{\rm ds}$ slope varies with the $V_{\rm gs}$. In order to improve the modeling accuracy, we propose

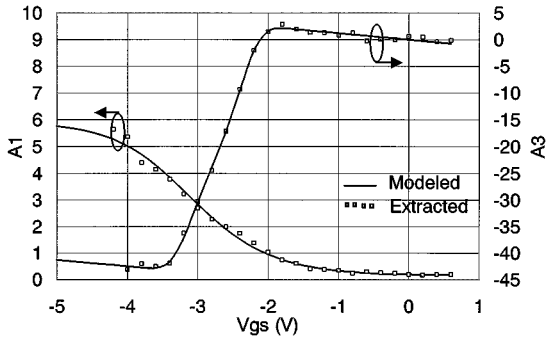

Fig. 5. The extracted A_1 and A_3 coefficients as functions of $V_{\rm gs}$.

an improved modeling function including the $V_{\rm gs}$ dependency of the F_2 as

$$G_{\rm ds}(V_{\rm gs}, V_{\rm ds}) = F_1(V_{\rm gs}, 0) \cdot F_2(V_{\rm gs}, V_{\rm ds}). \tag{5}$$

For the F_1, the hyperbolic tangent function represents the $V_{\rm gs}$ dependency of the $G_{\rm ds}$ and its derivatives [10] well at $V_{\rm ds} = 0$ V. The F_1 is shown by

$$F_1(V_{\rm gs}) \approx F_{\rm cnt} \cdot \Big[1 + \tanh(\psi)\Big] \tag{6}$$

where $F_{\rm cnt}$ is a modeled value at the center of the linear potion of the modeled value versus $V_{\rm gs}$ slope F_1–$V_{\rm gs}$, and the $V_{\rm gs}$ value at the $F_{\rm cnt}$ is $V_{\rm cnt}$. The ψ is a power series function centered at $F_{\rm cnt}$ with $V_{\rm gs}$ as a variable, and is shown by

$$\psi = P_1 \cdot (V_{\rm gs} - V_{\rm cnt}) + P_2 \cdot (V_{\rm gs} - V_{\rm cnt})^2 + P_3 \cdot (V_{\rm gs} - V_{\rm cnt})^3 + \cdots \tag{7}$$

where P_n, $n = 1, 2, 3, \cdots$ are the fitting parameters.

The F_2 represents the $V_{\rm ds}$ dependencies of the $G_{\rm ds}$ and its derivatives at each individual gate voltage, and is represented as

$$F_2(V_{\rm gs}, V_{\rm ds}) \approx 1 - \big[A_1(V_{\rm gs}) \cdot |V_{\rm ds}| + A_2(V_{\rm gs}) \cdot |V_{\rm ds}|^2 + A_3(V_{\rm gs}) \cdot |V_{\rm ds}|^3 + \cdots\big] \tag{8}$$

where, $A_n(V_{\rm gs})$, $n = 1, 2, 3, \cdots$ are $V_{\rm gs}$-dependent fitting coefficients. The extracted A_1 and A_3 coefficients from the 800-μm MESFET are shown in Fig. 5. A_2 and higher terms A_4, A_5, $\cdots$ became almost zero; hence, we neglected them. From the figure, the $A_1(V_{\rm gs})$ can be represented by (6). The $A_3(V_{\rm gs})$ is also represented by a modified modeling function of (6), and is shown by

$$A_3(V_{\rm gs}) \approx F_{\rm cnt} \cdot \Big[(1 + \lambda V_{\rm gs}) + \tanh(\psi)\Big] \tag{9}$$

where λ is a modulation parameter of $V_{\rm gs}$ and is the same as the Curtice model. The modeled A_1 and A_3 parameters are also shown in Fig. 5.

The measured g_n of the 800-μm MESFET were represented by the improved modeling function. In order to obtain accurate representations of the g_n, we fitted the improved modeling function to the all higher terms of the measured g_n by adjusting the model parameters. The extracted parameters for the modeling function are shown in Table I. The measured and the modeled $g_n$are shown in Fig. 6, and excellent agreements are achieved.

TABLE I
EXTRACTED PARAMETERS FOR THE IMPROVED $G_{\rm ds}$ MODELING FUNCTION

Parameters	F_1 parameters	A_1 parameters	A_3 parameters
F_{cnt}	0.561 [S]	2.969	-23.655
P_1	0.449 [S/V]	-0.858	-1.425
P_2	0.127 [S/V^2]	0.051	-0.413
P_3	0.112 [S/V^3]	0.016	-2.466
V_{cnt}	-0.457 [V]	-3.049 [V]	-2.694 [V]
λ	-	-	0.051

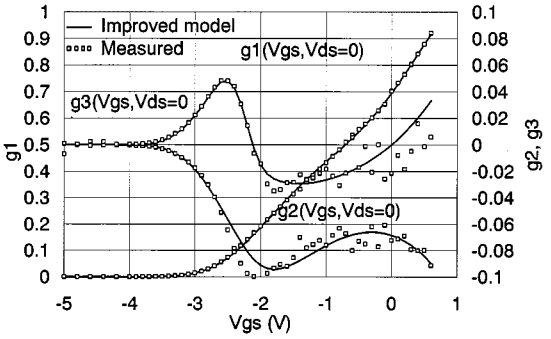

Fig. 6. Comparison of the measured and modeled g_n characteristics for an 800-μm MESFET.

The voltage dependencies of gate capacitors $C_{\rm gs}$ and $C_{\rm gd}$ play an important role in determining the high-frequency performance of MESFET's. Since the drain is unbiased in switching applications, these gate capacitors have identical gate voltage dependencies, and this phenomena can be represented by a modeling function. In the many modeling functions including the Curtice model [6]–[8], the gate capacitors are represented as the capacitor of the Scottky diodes [11] as follows:

$$C_{\rm gs}(V_{\rm gs}) = C_{\rm gd}(V_{\rm gd}) = \frac{C_{g0}}{\left(1 - \dfrac{V}{V_{bi}}\right)^m} \tag{10}$$

where C_{g0} is the zero-bias junction capacitance, V_{bi} is the built-in potential of the Schottky gate, m is a fitting parameter, and V is the intrinsic channel voltage. A conventional modeling function for the gate capacitors, shown in (10), is inadequate for gate voltages smaller than the pinchoff voltage since the conducting channel is totally depleted [12]. In order to improve the modeling accuracy, we propose an improved modeling function. Due to the similarity of $G_{\rm ds}(V_{\rm gs})$ and the gate capacitors, a modified modeling function of (6) was applied to represent the dependency on the gate voltage of the gate capacitors as

$$C_{\rm gs}(V_{\rm gs}) = C_{\rm gd}(V_{\rm gd}) \approx F_{\rm cnt} \cdot \Big[1 + C_f \cdot \tanh(\psi)\Big] \tag{11}$$

where

$$C_f = 1 - \frac{C_{g\,\min}}{F_{\rm cnt}} \tag{12}$$

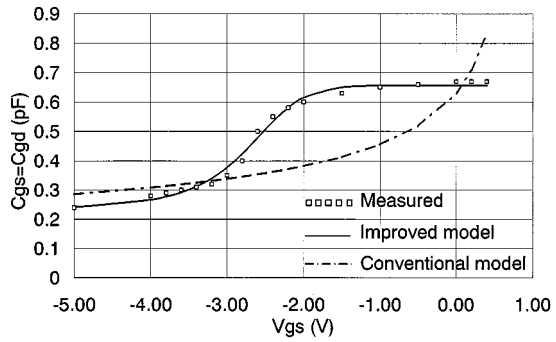

Fig. 7. Measured and modeled responses of the gate capacitors for an 800-μm MESFET. The parameters for the improved modeling function are $F_{\rm cnt} = 0.438$ pF, $C_{g\ \rm min} = 0.219$ pF, $V_{\rm cnt} = -2.748$ V, $P_1 = 1.217$, $P_2 = 0.364$, and $P_3 = 0.049$. The parameters for the conventional modeling function are $C_{g0} = 0.63$ pF, $V_{bi} = 0.8$ V, and $m = 0.40$.

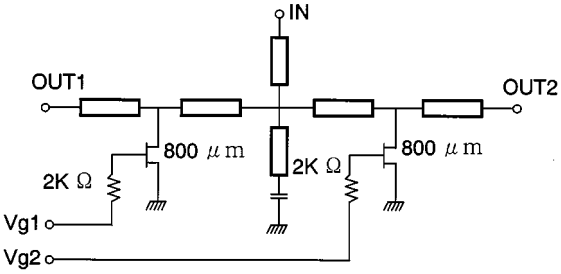

Fig. 8. Equivalent circuit of the MMIC SPDT switch.

and $C_{g\ \rm min}$ is the $C_{\rm gs}$ value at $V_{\rm gs} \ll V_p$.

Fig. 7 shows the comparison between the extracted and represented gate capacitors for the 800-μm MESFET. From the comparison, we recognize that the improved modeling function represents the gate voltage dependency over the large gate voltages with good accuracy.

V. Verification of the Improved Large-Signal Model

To verify the improved model's performance for the IMD power characteristic analyses, the characteristics calculated with the use of the improved model are compared with the experimental data taken from an MMIC SPDT switch. Small-signal simulation results are also compared with the experimental data to verify the performance of wide-band frequency applications. The MMIC SPDT switch was fabricated from a GaAs MMIC process optimized for switching applications. Fig. 8 shows an equivalent circuit of the MMIC SPDT switch. For large- and small-signal measurements, an RF signal was applied to the port "IN," and RF performance measurements were done at the port "OUT1." The port "OUT2" was terminated by a 50-Ω termination. The control voltages were $V_{g1} = 0$ V, $V_{g2} = -5$ V for an isolate state, and $V_{g1} = -5$ V, $V_{g2} = 0$ V for a transfer state.

A. Verification of the IMD Power Characteristic Analyses

Fig. 9(a) and (b) show the measured transfer and isolate state IMD power characteristics of the MMIC SPDT switch and the predicted IMD power characteristics for the improved and Curtice models. The IMD power characteristics were measured by

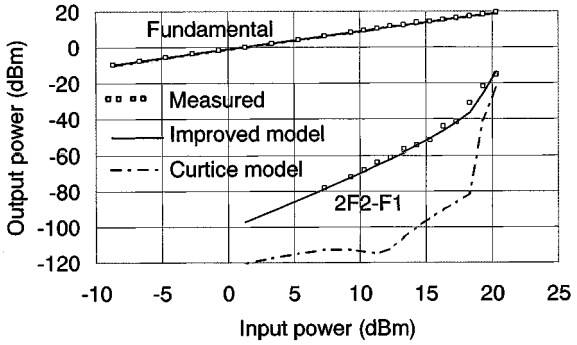

(a)

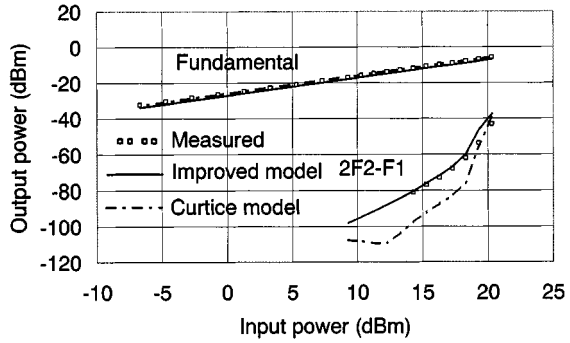

(b)

Fig. 9. IMD power of the MMIC SPDT switch. $F1 = 10.0$ GHz and $F2 = 10.1$ GHz. (a) Transfer state. (b) Isolate state.

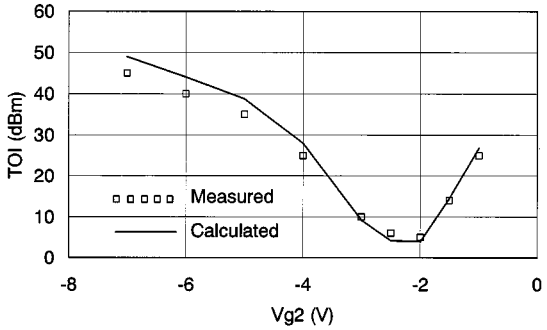

Fig. 10. Measured and simulated TOI point as a function of V_{g2} at the transfer state ($V_{g1} = 0$ V, $V_{g2} = -7$ to -1 V). The TOI was measured by the relationship from 10.0 to 10.1 GHz.

the relationship from 10.0 to 10.1 GHz. The predicted results of the improved model agree well with the measured data. However, the predicted results using the Curtice model show significant discrepancies between the measurements and predictions.

To verify the accuracy of the model at different gate voltages, third-order intercept (TOI) points were measured as a function of the control voltage V_{g2} and compared with the predicted performance from the improved model. Fig. 10 shows a comparison result, and very good agreement is achieved.

B. Verification of the Small-Signal Analysis

The predicted small-signal performances from the improved model agree well with the measured performances. Fig. 11(a) and (b) show the measured transfer and isolation state small-

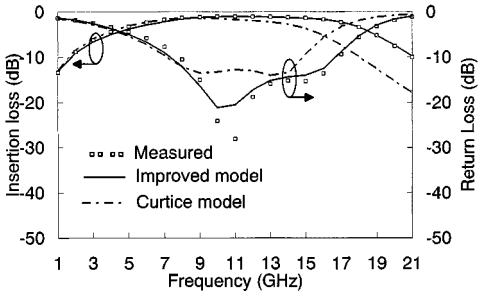

(a)

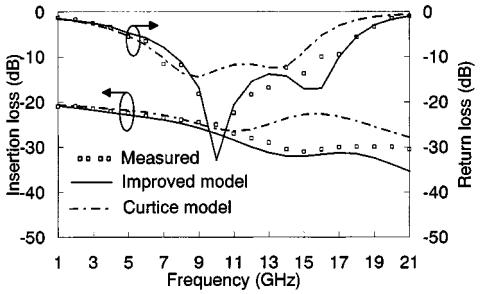

(b)

Fig. 11. Comparison of the measured and calculated small-signal responses for the MMIC SPDT switch. (a) Transfer state. (b) Isolate state.

signal performances of the MMIC SPDT switch and the predicted performances for the improved model, as well as the Curtice mode using the conventional modeling function for the gate capacitors. A dramatic improvement in the high-frequency performance prediction of the measured data is accomplished by using the improved model since the improved modeling function for the gate capacitor is applied to the improved model.

VI. Conclusion

The practical and accurate large-signal MESFET model and its parameter-extraction procedures for switching applications have been proposed. The small-signal drain current has been described as a function of the voltage-dependent drain conductance and its derivatives. The voltage-dependent drain conductance and its derivatives including gate capacitors have been represented by the improved modeling functions. The improved modeling function has been applied to predict the MMIC SPDT switch's performances, and has been compared to the measured performances. The results verified that the improved model is useful for both large- and small-signal circuit analyses for MESFET's in the control circuit applications.

References

[1] J. A. Pla and W. Struble, "Nonlinear model for predicting intermodulation distortion in GaAs FET RF switch devices," in *IEEE MTT-S Int. Microwave Symp. Dig.*, 1993, pp. 641–644.

[2] R. S. Virk and S. A. Mass, "Modeling MESFET's for intermodulation analysis in RF switches," *IEEE Microwave Guided Wave Lett.*, vol. 4, pp. 376–378, Nov. 1994.

[3] S. A. Maas and D. Neilson, "Modeling MESFET's for intermodulation analysis of mixers and amplifiers," *IEEE Trans. Microwave Theory Tech.*, vol. 38, pp. 1964–1971, Dec. 1990.

[4] G. Dambrine *et al.*, "A new method for determining the FET small-signal equivalent circuit," *IEEE Trans. Microwave Theory Tech.*, vol. 36, pp. 1152–1159, July 1988.

[5] J. M. Golio, *GASMAP Gallium Arsenide Model Analysis Programs Software and User's Manual*. Norwood, MA: Artech House, 1991.

[6] W. R. Curtice, "A MESFET model for use in the design of GaAs integrated circuits," *IEEE Trans. Microwave Theory Tech.*, vol. MTT-28, pp. 448–455, May 1980.

[7] A. Materka and T. Kacprazak, "Computer calculation of large-signal GaAs FET amplifier characteristics," *IEEE Trans. Microwave Theory Tech.*, vol. MTT-33, pp. 129–135, Feb. 1985.

[8] A. McCamant, G. McCormac, and D. Smith, "An improved GaAs FET device and circuit simulation in SPICE," *IEEE Trans. Microwave Theory Tech.*, vol. 38, pp. 822–824, June 1990.

[9] W. R. Curtice and M. Ettenberg, "A nonlinear GaAs FET model for use in the design of output circuits for power amplifiers," *IEEE Trans. Microwave Theory Tech.*, vol. 40, pp. 258–2266, Dec. 1992.

[10] I. Angelov, H. Zerbert, and N. Rorsman, "A new empirical nonlinear model for HEMT and MESFET devices," *IEEE Trans. Microwave Theory Tech.*, vol. MTT-33, pp. 129–135, Feb. 1985.

[11] S. M. Sze, *Physics of Semiconductor Devices*. New York: Wiley, 1969.

[12] T.-H. Chen and M. S. Shur, "A capacitance model for GaAs MESFET's," *IEEE Trans. Electron Devices*, vol. ED-12, pp. 883–891, May 1985.

Kohei Fujii graduated from the Junior Technical College of Electro-Communications, Tokyo, Japan, in 1984.

In 1980, he joined the Japan Radio Company Ltd., Tokyo, Japan. Since 1984, he has been in charge of development of microwave integrated circuits (MIC's) and MMIC's for radar systems. From 1994 to 1995, he studied the nonlinear modeling for GaAs devices as a Fellow Researcher at Washington University, St. Louis, MO. His current research interests are nonlinear modeling for microwave semiconductors and MMIC design.

Yasuhiko Hara received the B.E. and M.E. degrees from Sophia University, Tokyo, Japan, in 1976 and 1978, respectively.

In 1978, he joined the Japan Radio Company Ltd., Tokyo, Japan, where he has been in charge of development of active phased-array radar systems. He is currently a Director in the Radar Engineering Section.

Mr. Hara is a Registered Professional Engineer in Japan.

Toshiyuki Yakabe (M'89) received the B.E. and M.E. degrees in electric engineering from the Tokyo Metropolitan University, Tokyo, Japan, in 1980 and 1982, respectively, and the D. Eng. degree from Tohoku University, Sendai, Japan, in 1995.

From 1982 to 1985, he was with the Industrial Research Institute of Kanagawa Prefecture, Yokohama, Japan, where he was involved in automatic control measurement systems using microcomputers. From 1985 to 1987, he was with the Junior Technical College of Electro-Communications, Tokyo, Japan. He is currently an Assistant Professor in the Department of Information and Communication Engineering, University of Electro-Communications, Tokyo, Japan. His research interests are six-port technology, microwave instrumentation, and nonlinear modeling for microwave semiconductors.

Hatsuo Yabe (M'72) was born on February 5, 1937. He received the B.S. degree in communication engineering from the University of Electro-Communications, Tokyo, Japan, in 1960, and the Dr. Eng. degree from Tohoku University, Sendai, Japan, in 1984.

From 1963 to 1969, he served as a Research Associate in the Department of Communication Engineering, University of Electro-Communications, Tokyo, Japan, and is currently a Professor of information and communication engineering and serves as the Director of the university library since 1998. Since 1963, most of his research work has been concerned with waveguide twists. His current fields of investigation also include numerical methods for electromagnetic fields, microwave measurement systems, microwave electronics circuits, and electromagnetic compatibility.

Dr. Yabe is on the editorial board of the IEEE TRANSACTIONS ON MICROWAVE THEORY AND TECHNIQUES.